Journal of Crystal Growth 312 (2010) 3438–3442

Contents lists available at ScienceDirect

Journal of Crystal Growth

journal homepage: www.elsevier.com/locate/jcrysgro

MOCVD growth and optical properties of non-polar (1 1–2 0) *a*-plane GaN on (1 0–1 2) *r*-plane sapphire substrate

Hongbo Yu [a,*], Mustafa Ozturk [a], Pakize Demirel [a], Huseyin Cakmak [a], Ekmel Ozbay [a,b,c]

[a] Nanotechnology Research Center, Bilkent University, Bilkent, 06800 Ankara, Turkey
[b] Department of Physics, Bilkent University, Bilkent, 06800 Ankara, Turkey
[c] Department of Electrical and Electronics Engineering, Bilkent University, Bilkent, 06800 Ankara, Turkey

ARTICLE INFO

Article history:
Received 28 May 2010
Received in revised form
7 August 2010
Accepted 27 August 2010
Communicated by R. Fornari
Available online 28 September 2010

Keywords:
A1. Atomic force microscopy
A1. Crystal structure
A1. X-ray diffraction
A3. Metalorganic vapor phase epitaxy
B1. Nitrides
B2. Semiconducting gallium compounds

ABSTRACT

Non-polar *a*-plane GaN film with crystalline quality and anisotropy improvement is grown by use of high temperature AlN/AlGaN buffer, which is directly deposited on *r*-plane sapphire by pulse flows. Compared to the *a*-plane GaN grown on AlN buffer, X-ray rocking curve analysis reveals a remarkable reduction in the full width at half maximum, both on-axis and off-axis. Atomic force microscopy image exhibits a fully coalesced pit-free surface morphology with low root-mean-square roughness (~1.5 nm). Photoluminescence is carried out on the *a*-plane GaN grown on *r*-plane sapphire. It is found that, at low temperature, the dominant emission at ~3.42 eV is composed of two separate peaks with different characteristics, which provide explanations for the controversial attributions of this peak in previous studies.

1. Introduction

In recent years, non-polar and semi-polar planes of III-nitride have attracted much attention because of the benefits of completely or partially avoiding the polarization-induced electric fields along the *c*-axis [1–5]. Specially, *a*-plane (1 1–2 0) GaN film and heterostructures grown on *r*-plane (1 0–1 2) sapphire have great potential due to the high thermal stability, low price, and technological maturity of the sapphire substrate. However, planar *a*-plane GaN film grown on *r*-plane sapphire still suffers from very high density of crystal defects, such as threading dislocations (TDs) and basal-plane stacking faults (BSFs) [6,7], which deteriorate device performance and reduce the light emitting efficiency.

In order to improve the crystal quality of the *a*-plane GaN film, AlN and GaN nucleation or buffer layers were used and optimized [2,8–10], similar to the *c*-plane GaN growth [11,12]. Recently, Dai et al. [13] reported that the low temperature AlGaN nucleation layer showed superior properties than those of the AlN and GaN nucleation layer due to the reduction in lattice mismatch with the *r*-plane sapphire and *a*-plane GaN. However, little work has been reported on the growth of high temperature AlN/AlGaN on *r*-plane sapphire substrates as a buffer for subsequent GaN growth.

In the present study, we demonstrate the growth of high temperature AlN/AlGaN structure by novel pulse flows, and comparatively investigate the effects of AlN/AlGaN and AlN buffer layers on the crystalline quality of *a*-plane GaN films. The optical properties of *a*-plane GaN were also studied by photoluminescence (PL) characterizations.

2. Experimental details

The samples were all grown on double-polished (1–1 0 2) *r*-plane sapphire by a low-pressure metalorganic chemical vapor deposition (MOCVD) technique. Trimethylgallium (TMGa), trimethylaluminium (TMAl), and NH_3 were used as the precursors for Ga, Al, and N, respectively. Initially, the sapphire substrate was annealed at 1050 °C for 10 min in order to remove the surface contaminants. Then, 250 nm-thick (1 1–2 0) *a*-plane AlN and AlN/AlGaN films were directly grown on *r*-plane sapphire as a buffer for subsequent GaN growth. Fig. 1 shows the gas flow sequences that were used for the AlN and AlN/AlGaN structure growths. For the AlN film (sample A), TMAl flow was continuous during the NH_3 pulse-flow sequence, similar to the previous report [14]. For sample B, the NH_3 and TMGa sources were simultaneously supplied by pulse flows while the TMAl flow was continuous, which results in an AlN/AlGaN multilayer structure. The MOCVD growth pressure, temperature, and V/III ratio were controlled to

* Corresponding author. Tel.: +90 312 290 1024; fax: +90 312 290 1015.
E-mail addresses: yuhongbows@gmail.com, hongboyu@bilkent.edu.tr (H. Yu).

0022-0248/$ - see front matter © 2010 Elsevier B.V. All rights reserved.
doi:10.1016/j.jcrysgro.2010.08.052

be 50 mbar, 1100 °C, and 230, respectively, for the growth of sample A. Sample B was grown with the V/III ratio of 400, while other growth parameters, such as growth pressure and temperature were the same as those of sample A. The growth rates for AlN and AlN/AlGaN structures were 5.0 and 7.2 nm/min, respectively. After the growth of the buffer layers, 4 μm-thick *a*-plane GaN films were grown on the two kinds of buffers at 1050 °C. In the first step, a relatively high V/III ratio (1500) and reactor pressure (300 mbar) were applied for 10 min, in order to enable the GaN growth to start from a three-dimensional (3D) mode. Subsequently, the V/III molar ratio and reactor pressure were reduced to 200 and 100 mbar, respectively, which resulted in a fully coalesced surface [15]. A high-resolution X-ray diffractometer (Rigaku-Smartlab) was employed to evaluate the crystalline quality and anisotropy of the samples, delivering a CuKa1 line of wavelength λ=0.1541 nm. X-ray rocking curves (XRCs) were measured for the on-axis and off-axis diffraction planes. Surface morphology of the samples was examined by atomic force microscopy (AFM), Veeco DI-CP II, using contact mode. Optical properties of the epi-layers were investigated by UV optical transmission spectroscopy and temperature-dependent PL, using a 325 nm He–Cd laser.

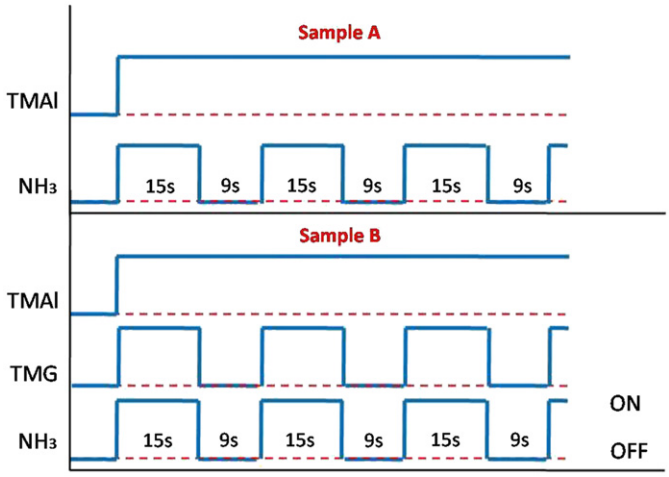

Fig. 1. Schematics of the NH_3, TMAl, and TMGa flow sequence for the growths of AlN and AlN/AlGaN buffer layers on *r*-plane sapphire.

3. Results and discussion

Fig. 2a and b shows the AFM images of as-grown samples A and B, respectively. Both samples feature an anisotropy stripe-like mosaic surface morphology, elongated along the *c*-axis. This is possibly due to the asymmetric lattice mismatch between *r*-plane sapphire and *a*-plane Al(Ga)N along the *m*-axis and *c*-axis [13]. The root-mean-square (RMS) surface roughness of sample A was measured as 1.98 nm over the 5×5 μm^2 scan area. The RMS surface roughness of sample B was significantly reduced to 1.21 nm over the same scan area, which is indicative of improved surface smoothness. Moreover, mean size of the sub-grain for sample B was remarkable larger than that of sample A, which might be due to the enhancement of the lateral migration of Ga atoms compared to Al atoms on the growing surface. In general, large grain size is desirable for an epilayer with a mosaic structure, because the majority of dislocations in the epilayer are formed at grain boundaries [16,17]. The relatively smooth surface as well as large grain dimension of AlN/AlGaN buffer supplies a superior underlying layer for the subsequent growth of *a*-plane GaN film.

Optical transmission was carried out for both the samples grown under various processing conditions. As shown in Fig. 3, curves I and II correspond to the spectrum of samples A and B, respectively. The spectrum of sample A shows the optical transmission starting from 203 nm, which corresponds to the band gap of the AlN film. Compared to the spectrum of sample A, a higher rate of transmission along with well-defined Fabry–Perot oscillations was clearly observed in the spectrum of sample B, due to the improved crystalline quality and smoother surface. The cut-off wavelength of sample B is measured as ~220 nm, which corresponds to ~85% Al content in the AlGaN alloy.

Specular GaN films were grown on the AlN and AlN/AlGaN buffers, which are named as samples C and D, respectively. Fig. 4 shows AFM images of samples C and D over 5×5 μm^2 scan area. Both samples exhibited a fully coalesced pit-free surface under the AFM characterizations. Anisotropy stripe features along the *c*-direction and surface undulation along the *m*-direction were observed on both of the samples, which is similar to the previous report [2,8,11]. The RMS roughness of samples C and D was measured as 1.94 and 1.52 nm, respectively, indicating the improvement of surface smoothness by the use of high quality AlN/AlGaN buffer.

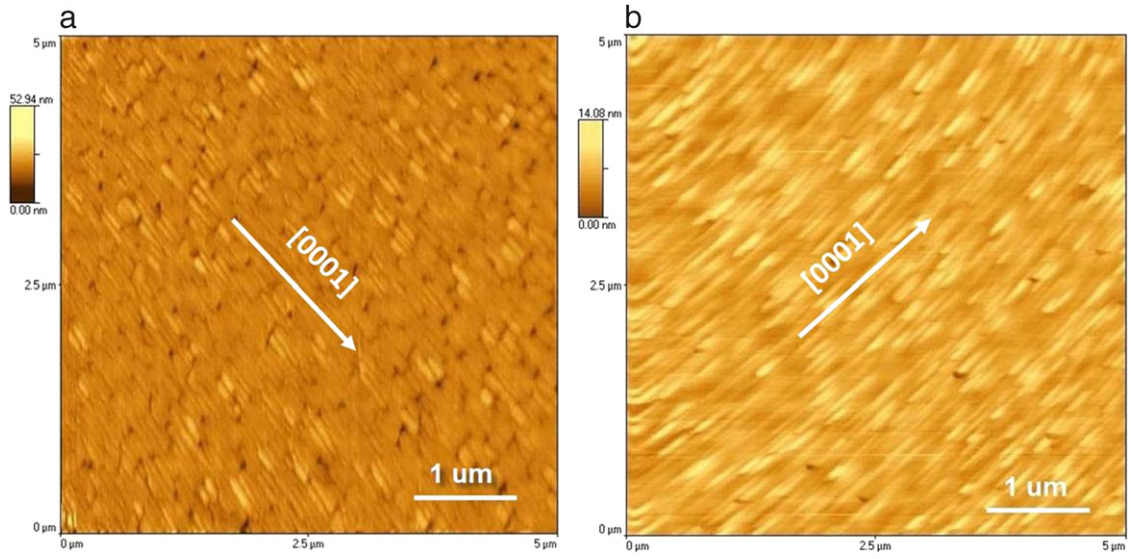

Fig. 2. The 5 μm × 5 μm AFM images of 250 nm-thick AlN (a) and AlN/AlGaN (b) structures on *r*-plane sapphire.

Fig. 5 shows FWHMs of the on-axis (1 1–2 0) XRCs as a function of azimuthal angle, φ, which is set as 0° (*c*-axis [0 0 0 1]) and 90° (as shown in Fig. 4b) when the incident and diffracted X-ray beam is parallel and perpendicular to the stripe direction of the GaN film, respectively. FWHM of the on-axis (1 1–2 0) XRCs increases monotonically with angle φ turning from 0° to 90°, and then decreases symmetrically with angle φ turning from 90° to 180° for samples C and D. As shown in Fig. 5, the FWHMs of XRCs for sample D are remarkably lower than those for sample C in the measurement region. In addition, both the samples exhibit anisotropic FWHMs for the on-axis XRCs, which might be due to the stripe-like structure originating from the asymmetric lattice mismatch and the adatom diffusion length. The ratios of the maximum (φ=90°) to the minimum (φ=0°) FWHMs are calculated as 1.51 and 1.29 for samples C and D, respectively, indicating the improvement of isotropy by using the high temperature AlN/AlGaN buffer.

Thin films grown on substrates with lattice mismatches usually exhibit a mosaic structure, which means that the films consist of sub-grains slightly mis-oriented with respect to each other and the underlying substrate. The FWHM of on-axis (1 1–2 0) XRCs is an effective means of evaluating the mosaic tilt (out-of-plane misalignment) in the epi-layer. However, it is not sensitive to the mosaic twist (in-plane misalignment), which is an important aspect of the mosaic structure. To study the mosaic tilt/twist distribution in the *a*-plane GaN film, we further carried out XRD research on the off-axis planes, such as (3 0–3 0) and (−2 1 1 0) for φ=0° and (1 1–2 2) and (1 1–2 4) for φ=90° in this study. Fig. 6a and b shows FWHMs of the off-axis XRCs as a function of inclination angle, χ, with the azimuthal angle φ=0° and 90°, respectively. In both azimuthal directions, the FWHMs of off-axis XRCs display a lower value for sample D than those for sample C. Compared to those of sample C, sample D has remarkably low peak widths for both on-axis (Fig. 5) and off-axis (Fig. 6) reflections, indicating a significant improvement of crystalline quality and anisotropy through the application of the AlN/AlGaN buffer layer. For sample D, the FWHMs of on-axis (1 1–2 0) and off-axis (3 0–3 0) XRCs are measured as 0.165° and

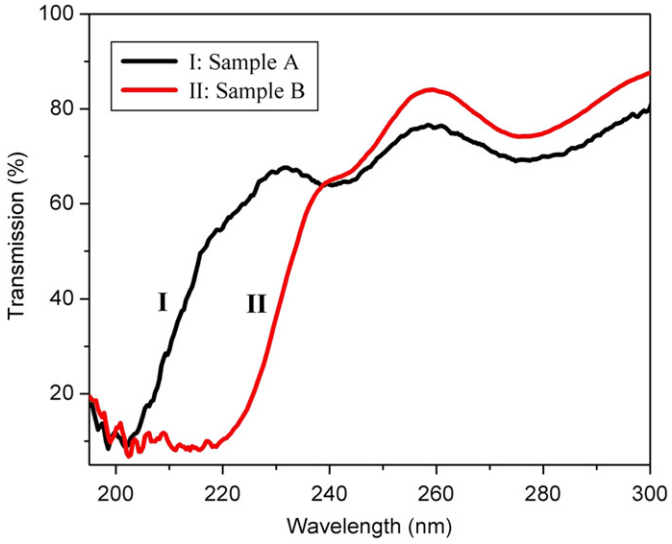

Fig. 3. UV transmission spectroscopy of the AlN and AlN/AlGaN structures grown on *r*-plane sapphire.

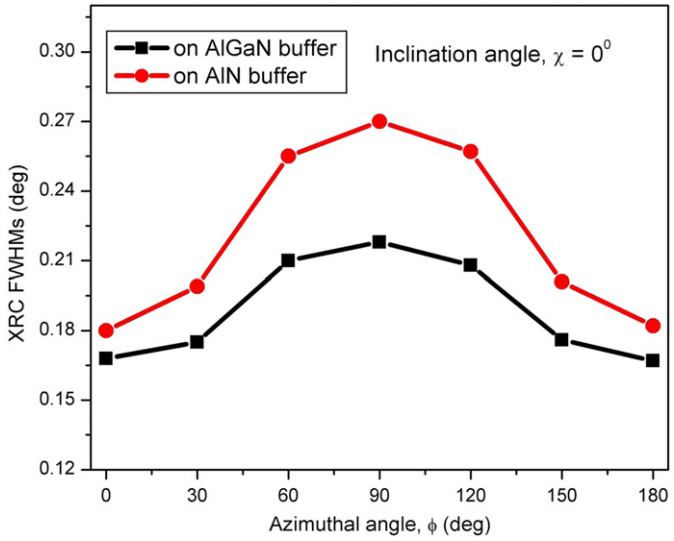

Fig. 5. FWHMs of the (11–20) on-axis XRCs for *a*-plane GaN as a function of azimuthal angle φ.

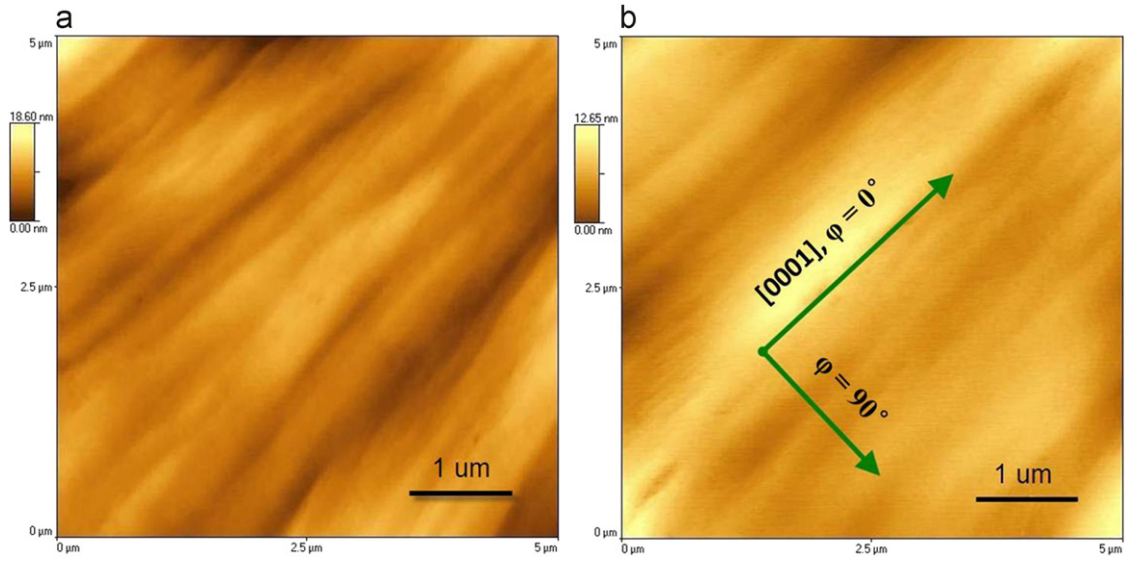

Fig. 4. The 5 μm × 5 μm AFM images of *a*-plane GaN films grown on AlN (a) and AlN/AlGaN (b) buffer.

0.269°, respectively, which are among the lowest values reported for *a*-plane GaN on *r*-plane sapphire without lateral epitaxial overgrown (LEO) process [15,18].

To investigate the optical properties of *a*-plane GaN, temperature-dependent PL was performed on the as-grown samples. PL spectra from samples C and D show a similar behavior. In this paper, we provide the PL investigations of sample D. Fig. 7a shows the 20 K PL spectrum of sample D as a black solid line. Seven emissions, peaked at approximately 3.112, 3.218, 3.300, 3.333, 3.419, 3.438, and 3.489 eV (labeled as 1–7), were well resolved using multiple Gaussian fitting functions. A good matching of the fitted curve (red dash line) with the experiment spectrum is helpful in identifying the emissions by determining the peak positions and FWHMs accurately. Separately, the peak at 3.489 eV

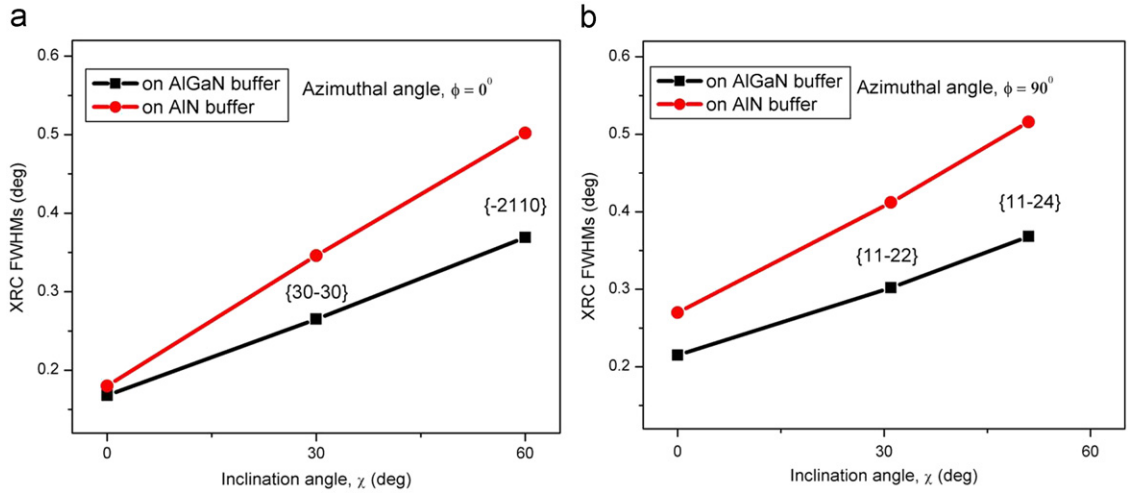

Fig. 6. FWHM of off-axis XRCs for *a*-plane GaN as a function of the plane inclination angle, χ, for two sets of planes at $\varphi=0^\circ$ (a) and $\varphi=90^\circ$ (b).

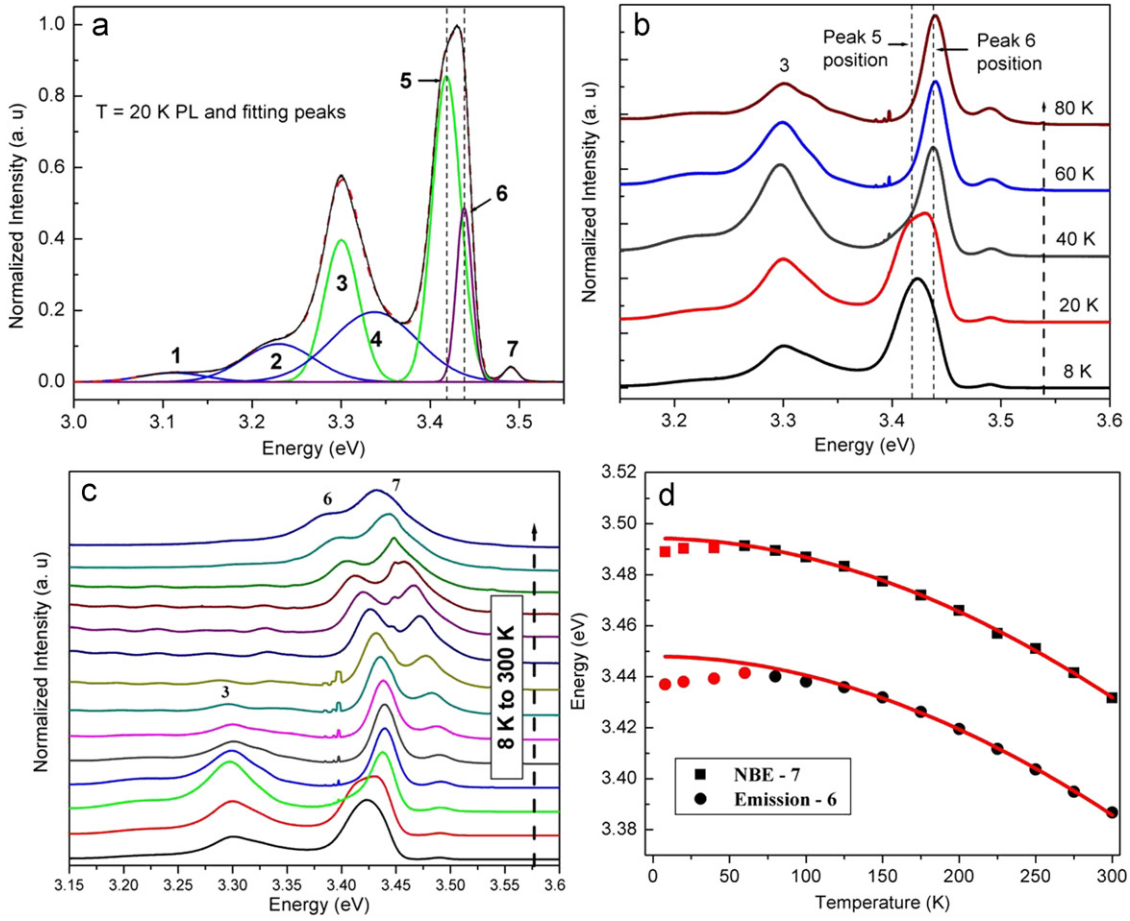

Fig. 7. PL characterizations of *a*-plane GaN grown on AlN/AlGaN multilayer buffer: (a) 20 K PL spectrum and the multiple Gaussian function fitting results, (b) detailed PL spectra in the temperature region of 8–80 K, the peak positions of peaks 5 and 6 were represented as dashed lines separately, (c) PL spectra measured in the temperature region 8–300 K, and (d) the peak energy positions of emissions 6 and 7 as a function of temperature.

(peak 7, FWHM=16.2 meV) is a common near band-edge emission (NBE), while the peak at 3.30 eV (FWHM=39.2 meV) has been generally attributed to the donor–acceptor pair (DAP) emission, as previously reported [19,20]. According to the energy separation, emissions 2 and 1 are assigned to the one to two longitudinal optical (LO) phonon replicas of emission 3.

Origin of the dominant peak at around 3.42 eV has not been well understood. In the previous studies, the emissions from approximately 3.41 to 3.44 eV were indiscriminately identified as a "near 3.4 eV emission", which were controversially attributed to BSFs-related DAP, quantum well formed in BSFs or exciton bound to BSFs [6,21–23]. Since *a*-plane GaN layers grown on *r*-plane sapphire contain a high density of BSFs [2,6,9], strong luminescence at around 3.4 eV is expected. In this research, it is found that this dominant peak with a relatively large width can be well fitted by two separate emissions at 3.419 and 3.438 eV with FWHMs of 32.7 and 16.8 meV, respectively. The two emissions show remarkably different characteristics with increasing the temperature. Compared to emission 6, emission 5 has a much higher density when the temperature is lower than 20 K (Fig. 7a), but it quenches very fast with increase in temperature, as shown in Fig. 7b. In contrast, emission 6 can be observed in the spectrum with temperature increasing to 300 K, as shown in Fig. 7c.

Fig. 7d shows the peak positions of the NBE and emission 6 as a function of temperature. Experimental points are fitted by Varshni's empirical formula: $E=E_0-\alpha T^2/(T+\beta)$. For the NBE emission, we obtained the best fit for $E(0)=3.493$ eV, $\alpha=0.82$ meV/K, and $\beta=857$ K, which are of similar values as in the report for *c*-plane GaN [24]. At low temperature, the excitons are essentially localized on donors (D^0X). With increase in temperature, the D^0X progressively quenches to the benefit of the *A* free exciton emission, in agreement with previous observations in *c*-plane GaN [25]. The energy peak position of emission 6 blueshifts with temperature increasing from 8 to ~80 K, and then it approximately follows the same redshift with exciton emission 7 above 80 K.

According to the behavior of emissions 5 and 6 as a function of temperature and FWHMs of the two peaks, we suggest that emission 5 is attributed to a recombination of a BSFs-related DAP [23,26]. Emission 6 is attributed to the recombination of the exciton bound to the BSFs [6,22,27]. Our experimental results show that at low temperature, there are two kinds of BSFs-related emissions existing simultaneously in the spectrum of *a*-plane GaN grown on *r*-plane sapphire, which may help to clarify the controversial attributions of the dominant emission.

In summary, this work has demonstrated the growth of AlN and AlN/AlGaN buffer layers on *r*-plane sapphire using the pulse-flow technique. Crystalline quality and anisotropy are improved in *a*-plane GaN films using high temperature AlN/AlGaN buffer. AFM image shows a fully coalesced pit-free surface with low RMS roughness (~ 1.5 nm). Temperature-dependent PL was carried out on *a*-plane GaN. It was first found that, at low temperature, the dominant peak at ~3.42 eV is composed of two separate peaks with different properties, which provide explanations for the controversial attributions of this peak in previous studies.

Acknowledgements

This work was supported by the European Union under the Projects EU-PHOME and EU-CONAM, and TUBITAK under Project nos. 107A004 and 107A012. One of the authors (E.O.) also acknowledges partial support from the Turkish Academy of Sciences.

References

[1] P. Waltereit, O. Brandt, A. Trampert, H.T. Grahn, J. Menniger, M. Ramsteiner, M. Reiche, K.H. Ploog, Nature (London) 406 (2000) 865.
[2] M.D. Craven, S.H. Lim, F. Wu, J.S. Speck, S.P. DenBaars, Appl. Phys. Lett. 81 (2002) 469.
[3] H. Yu, L.K. Lee, T. Jung, P.C. Ku, Appl. Phys. Lett. 90 (2007) 141906.
[4] T.J. Baker, B.A. Haskell, F. Wu, P.T. Fini, J.S. Speck, S. Nakamura, Jpn. J. Appl. Phys. 44 (2005) L920.
[5] H. Yu, T. Jung, P.C. Ku, Phys. Status Solidi C 5 (1618) 2008.
[6] R. Liu, A. Bell, F.A. Ponce, C.Q. Chen, J.W. Yang, M.A. Khan, Appl. Phys. Lett. 86 (2005) 021908.
[7] Z.H. Wu, A.M. Fischer, F.A. Ponce, B. Bastek, J. Christen, T. Wernicke, M. Weyers, M. Kneissl, Appl. Phys. Lett. 92 (2008) 171904.
[8] D.S. Li, H. Chen, H.B. Yu, X.H. Zheng, Q. Huang, J.M. Zhou, J. Cryst. Growth 265 (2004) 107.
[9] S. Chang, H. Yang, T. Lu, H. Kuo, S. Wang, J. Cryst. Growth 312 (2010) 1307.
[10] X. Ni, Y. Fu, Y.T. Moon, N. Biyikli, H. Morkoc, J. Cryst. Growth 290 (2006) 166.
[11] S. Nakamura, T. Mukai, M. Senoh, Appl. Phys. Lett 64 (1687) 1994.
[12] H. Yu, M.K. Ozturk, S. Ozcelik, E. Ozbay, J. Cryst. Growth 293 (2006) 273.
[13] J.N. Dai, Z.H. Wu, C.H. Yu, Q. Zhang, Y.Q. Sun, Y.K. Xiong, X.Y. Han, L.Z. Tong, Q.H. He, F.A. Ponce, C.Q. Chen, J. Electron. Mater. 38 (1938) 2009.
[14] H. Hirayama, T. Yatabe, N. Noguchi, T. Ohashi, N. Kamata, Appl. Phys. Lett. 91 (2007) 071901.
[15] Q. Sun, T. Ko, C.D. Yerino, Y. Zhang, I. Lee, J. Han, T. Lu, H. Kuo, S. Wang, Jpn. J. Appl. Phys. 48 (2009) 071002.
[16] F.A. Ponce, B.S. Krusor, J.S. Major Jr., W.E. Plano, D.F. Welch, Appl. Phys. Lett. 67 (1995) 410.
[17] A.E. Wickenden, D.D. Koleske, R.L. Henry, R.J. Gorman, J.C. Culbertson, M.E. Twigg, J. Electron. Mater. 28 (1999) 301.
[18] F. Ranalli, P.J. Parbrook, J. Bai, K.B. Lee, T. Wang, A.G. Cullis, Phys. Status Solidi C 6 (No. S2) (2009) S780.
[19] M. Narukawa, R. Miyagawa, B. Ma, H. Miyake, K. Hiramatsu, J. Cryst. Growth 311 (2009) 2903.
[20] P.P. Paskov, R. Schifano, B. Monemar, T. Paskova, S. Figge, D. Hommel, J. Appl. Lett. 98 (2005) 093519.
[21] P.P. Paskov, T. Paskova, B. Monemar, S. Figge, D. Hommel, B.A. Haskell, P.T. Fini, J.S. Speck, S. Nakamura, Superlattices Microstruct. 40 (2006) 253.
[22] D. Li, B. Ma, R. Miyagawa, W. Hu, M. Narukawa, H. Miyake, K. Hiramatsu, J. Cryst. Growth 311 (2009) 2906.
[23] H.B. Yu, H. Chen, D. Li, Y.J. Han, X.H. Zheng, Q. Huang, J.M. Zhou, J. Cryst. Growth 263 (2004) 94.
[24] I. Vurgaftman, J.R. Meyer, J. Appl. Phys. 94 (2003) 3675.
[25] S. Fischer, G. Steude, D.M. Hofmann, F. Kurth, F. Anders, M. Topf, B.K. Meyer, F. Bertram, M. Schmidt, J. Christen, L. Eckey, J. Holst, A. Hoffmann, B. Mensching, B. Rauschenbach, J. Cryst. Growth 189–190 (1998) 556.
[26] F. Calley, F.J. Sanchez, J.M.G. Tijero, M.A. Sanchez-Garcia, E. Callej, R. Beresford, Semicond. Sci. Technol. 12 (1997) 1396.
[27] Y.T. Rebane, Y.G. Shreter, M. Albrecht, Phys. Status Solidi A 164 (1997) 141.